THE JOURNAL OF COMPARATIVE NEUROLOGY 508:605–614 (2008)

Distribution of Neurofilament Proteins in the Lateral Geniculate Nucleus, Primary Visual Cortex, and Area MT of Adult *Cebus* Monkeys

JULIANA GUIMARÃES MARTINS SOARES, PAULO HENRIQUE ROSADO DE CASTRO, MARIO FIORANI, SHEILA NASCIMENTO-SILVA AND RICARDO GATTASS*
Instituto de Biofísica Carlos Chagas Filho, Universidade Federal do Rio de Janeiro, Rio de Janeiro, RJ, 21949-900, Brasil

ABSTRACT

We investigated the distribution pattern of SMI-32-immunopositive cells in the lateral geniculate nucleus (LGN) and in the primary (V1) and middle temporal (MT) cortical visual areas of the adult New World monkey *Cebus apella*. In the LGN, the reaction for SMI-32 labeled cells in both the magnocellular (M) and parvocellular (P) layers. However, the cellular label was heavier in M layers, which also showed a more intense labeling in the neuropil. In V1, the reaction showed a lamination pattern, with the heaviest labeling occurring in layer 4B and upper layer 6 (layers that project to area MT). Area MT shows a dense band of labeled neuropil and large pyramidal neurons in layer 3, large darkly labeled but less densely packed neurons in layer 5, and a population of small, lightly labeled cells in layer 6. These results resemble those found in other New and Old World monkeys, which suggest that the preferential labeling of projection neurons associated with fast-conducting pathways to the extrastriate dorsal stream is a common characteristic of simian primates. In the superficial layers of V1 in *Cebus* monkeys, however, SMI-32-labeled neurons are found in both cytochrome oxidase blobs and interblob regions. In this aspect, our results in *Cebus* are similar to those found in the Old World monkey *Macaca* and different from those described for squirrel monkey, a smaller New World Monkey. In *Cebus*, as well as in *Macaca*, there is no correlation between SMI-32 distribution and the blob pattern. J. Comp. Neurol. 508:605–614, 2008.

Indexing terms: SMI-32 monoclonal antibody; pyramidal neuron; visual system; primate

SMI-32 is a monoclonal antibody that recognizes nonphosphorylated neurofilaments (N-NF) distributed throughout the somata, the dendrites, and at least the proximal axons of certain neurons (Sternberger and Sternberger, 1983). Previous studies have shown that SMI-32-immunoreactive (SMI-32-ir) neurons represent a subset of pyramidal neurons, with long axonal projections. In the cerebral cortex, immunoreactivity to N-NF protein was not observed in nonpyramidal neurons, except for the large multipolar layer 4B neurons and the smaller bitufted layer 3 neurons in primary visual area (V1) (Campbell and Morrison, 1989; Hof and Morrison, 1990, 1995).

In the dorsal lateral geniculate nucleus (LGN) of primates, a stronger expression of N-NF protein was observed in the magnocellular layers, compared with the parvocellular layers (Chaudhuri et al., 1996; Bourne and Rosa, 2003). A differential distribution of SMI-32-ir neurons was also observed across cortical areas (Campbell and Morrison, 1989; Hof and Morrison, 1995; Chaudhuri

Grant sponsor: Programa de Apolo a Núcleos de Excelência; Grant sponsor: Conselho Nacional de Desenvolvimento Científico e Tecnológico; Grant sponsor: Financiadora de Estudos e Projetos; Grant sponsor: Fundaçáo de Amparo à Pesquisa do Estado do Rio de Janeiro.

*Correspondence to: Ricardo Gattass, Instituto de Biofísica Carlos Chagas Filho, Bloco G, CCS, UFRJ, Ilha do Fundão, Rio de Janeiro, RJ, 21941-902, Brasil. E-mail: rgattass@biof.ufrj.br.

Received 19 September 2007; Revised 21 December 2007; 13 February 2008

DOI 10.1002/cne.21718

Published online in Wiley InterScience (www.interscience.wiley.com).

et al., 1996; Bourne and Rosa, 2003; Baldauf, 2005; Van der Gucht et al., 2005, 2006). In macaque monkey, visual areas related to the magnocellular system in the superior temporal sulcus (STS) and parietal cortices are all characterized by the presence of very large SMI-32-ir neurons in layer 5A. Conversely, areas related to the parvocellular system, including V4 and the inferior temporal cortex, show a denser but more heterogeneous population of smaller and lightly stained neurons. In area V1, the most prominent feature is the presence of densely labeled cells in layer 4B and at the interface between layers 5 and 6 (Hof and Morrison, 1995). These cells are a component of the magnocellular system projecting from area V1 to area MT (Spatz, 1977; Fries et al., 1985; Shipp and Zeki, 1989; Rosa et al., 1993).

A previous study in *Macaca* showed that whereas SMI-32-ir apical dendrites bundle together in small clusters in the superficial layers of V1, labeled neurons are scattered across both cytochrome oxidase (CO) blob and interblob domains (Fenstemaker et al., 2001). In contrast, in squirrel monkeys, the density of SMI-32-labeled neurons was found to be greater within the CO interblobs than in the blobs (Duffy and Livingstone, 2003).

In the present paper we report on the distribution of neurofilament protein in LGN and in cortical visual areas V1 and MT of *Cebus apella*. We compare our results with those described in *Macaca* as well as in squirrel monkey (Duffy and Livingstone, 2003) and marmoset (Bourne and Rosa, 2003; Bourne et al., 2007). Smaller New World monkeys like marmoset show a weaker degree of laminar organization in the LGN and a lack or weaker degree of eye input segregation in layer 4 in the primary visual cortex. On the other hand, in both *Cebus* and macaque, the LGN is divided into paired magnocellular and parvocellular layers, with the parvocellular layers further subdivided into leaflets, and has clear ocular dominance columns (Spatz, 1978; Kaas et al., 1978; Hendrickson et al., 1978; Hess and Edwards, 1987; Rosa, 2002; Bourne and Rosa, 2003).

When we take into consideration brain size and sulcal pattern, as well as relative position of homologous visual areas, we find that the *Cebus* is comparable to the Old World monkey *Macaca* (Gattass and Gross, 1981; Gattass et al., 1981, 1987, 2005; Rosa et al., 1988; Fiorani et al., 1989). The similarities between *Cebus* and *Macaca* were also highlighted in a recent study (Padberg et al., 2007) of the cortical parietal areas that process inputs from the hand. In contrast, in smaller New World monkeys, fewer cortical fields are present in the corresponding parietal location. It has been suggested that there are differences in the chemoarchitectural pattern even between members of the same order and that these are important in tracing evolutionary adaptations and phylogenetic relationships (Bourne et al., 2007). Thus, the present study, on the distribution of neurofilament protein in the LGN and in areas V1 and MT in *Cebus*, will allow comparison of the cytochemical organization of these structures in New and Old World monkeys.

MATERIALS AND METHODS

In this study we used six young adult *Cebus apella* monkeys of both sexes, weighing between 2.5 and 3.7 kg. All experimental protocols were conducted following the NIH guidelines for animal research, and they were approved by the Committee for Animal Care and Use of the Instituto de Biofísica Carlos Chagas Filho, UFRJ. These animals were also used in other immunocytochemistry studies in our laboratory.

Four of these animals were deeply anesthetized with sodium pentobarbital (30 mg/kg) and perfused transcardially with normal saline followed by 4% paraformaldehyde in phosphate-buffered saline (PBS); 4% paraformaldehyde in PBS + 2.5% glycerol; PBS + 5% glycerol; and PBS + 10% glycerol. Serial 40-μm-thick, coronal (two animals) or parasagittal (two animals) sections of the brains were obtained by using a cryostat. Adjacent series were stained for cell bodies with cresyl violet and for myelin by the Gallyas technique (Gallyas, 1979) and then reacted for cytochrome oxidase (CO) histochemistry (Silverman and Tootell, 1987) or for immunocytochemistry for SMI-32. For the remaining two animals, after perfusion with saline, the brains were removed from the skull, and the block with area V1 was flattened, fixed with the same solutions used for the previous animals, and sectioned parallel to the pial surface at 50 μm. Adjacent series were reacted for CO and for immunocytochemistry for SMI-32.

The SMI-32 monoclonal antibody to neurofilaments (SMI 32, Sternberger Monoclonals, Baltimore, MD) is a mouse monoclonal IgG1 that reacts with a nonphosphorylated epitope in neurofilament H of most mammalian species. This antibody labels neuronal cell bodies, dendrites, and some thick axons in the central and peripheral nervous systems (Sternberger and Sternberger, 1983; Campbell and Morrison, 1989).

For immunocytochemical reactions, free-floating sections were washed in PBS and incubated overnight with SMI-32 (1:4,000) in a solution containing 0.05% bovine serum albumin and 0.3% Triton X-100 in 0.001 M PBS, pH 7.4, at room temperature. They were then incubated for an additional hour in biotinylated anti-mouse secondary antibody (1:200) and then processed by the avidin-biotin method with ABC kits (Vector, Burlingame, CA) and nickel-enhanced diaminobenzidine. The sections were rinsed in PBS, mounted on gelatin-coated slides, dehydrated, and coverslipped. Control sections were prepared by omitting the primary antibody in the incubation solution. These sections showed no specific staining. Sections were examined under brightfield microscopy and photomicrographed by using a Zeiss Axiocam attached to the microscope. Adobe Photoshop 6 was used to enhance image contrast and to crop and size the images for illustration (Adobe Systems, San Jose, CA).

The study of the distribution pattern of SMI-32-ir cells in layers 2/3 was performed in four flattened hemispheres. The labeled cells were plotted in three parafoveal sections of 3 mm^2 for each hemisphere, under high magnification, by using the Neurolucida system (MicroBrightField, Williston, VT).

The CO blobs were identified with the aid of densitometric analysis by means of a Matlab routine. First the low-pass Fourier-filtered (1.1 cycles/mm) image was subtracted from the original image, and then the image was blurred with a Gaussian filter (σ = 100 μm). Then the borders of CO blobs were delineated at 0.4 of the maximum to minimum optical density, in order to obtain an area between 30 and 33% of the total area corresponding to blobs. The drawings of the CO blobs were superposed with adjacent sections reacted for SMI-32, and the cell density was measured in blob and interblob regions. The data obtained for blob and interblobs regions were statistically compared by using t-test analysis.

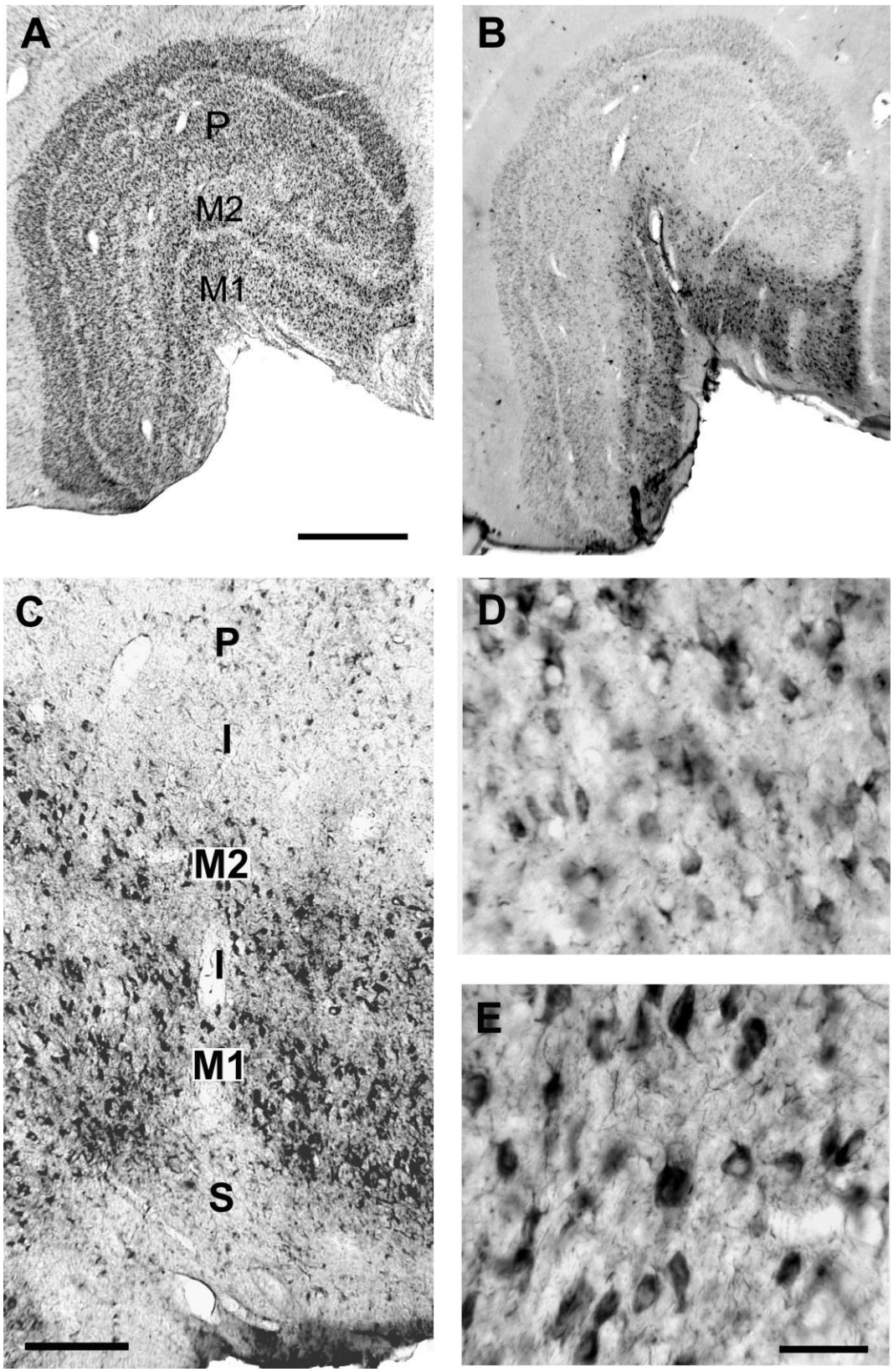

Fig. 1. Photomicrographs of coronal sections of the lateral geniculate nucleus of *Cebus*. **A:** Section of the LGN stained by the Nissl method showing the magnocellular (M1 and M2) and parvocellular (P) layers. **B:** Section adjacent to that illustrated in A reacted for SMI-32, showing a more intense reaction in M layers. **C:** Photomicrograph in an intermediate magnification showing S, M, interlaminar (I), and P layers. **D,E:** Enlarged photomicrographs illustrating SMI-32-ir cells in magnocellular (D) and parvocellular (E) layers. Scale bar = 1 mm in A (applies to A,B); 200 μm in C; 50 μm in E (applies to D,E).

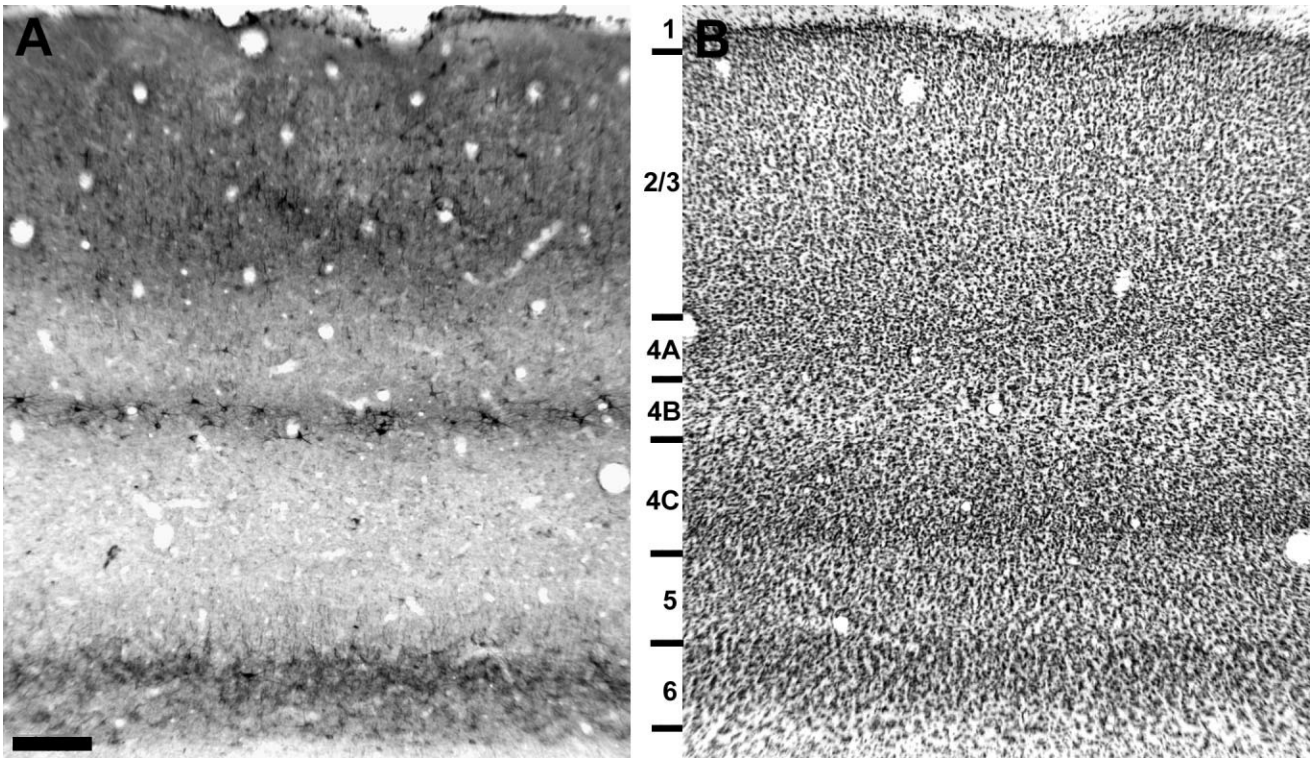

Fig. 2. Photomicrographs of adjacent coronal sections of V1 in *Cebus* monkey. **A:** Section stained by immunocytochemistry for SMI-32 showing the lamination pattern presented by neurofilament proteins in V1. **B:** Adjacent section stained by the Nissl method, with the approximate limits of the layers are indicated. Scale bar = 200 μm in A (applies to A,B).

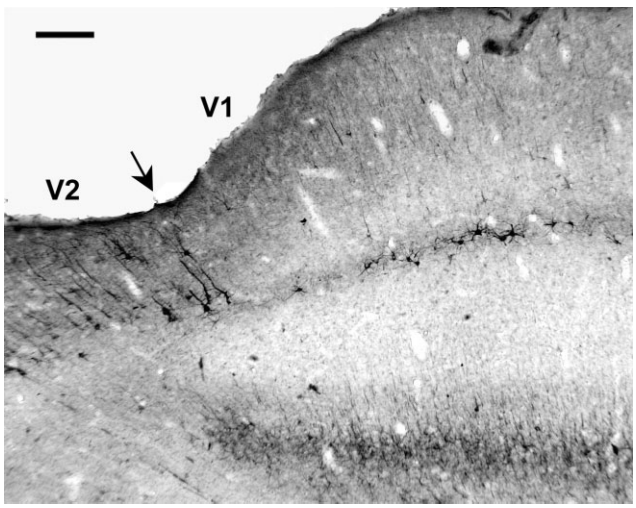

Fig. 3. Photomicrograph of a coronal section of V1 in *Cebus* monkey, stained by immunocytochemistry for SMI-32 showing the V1/V2 border (arrow). Scale bar = 200 μm.

RESULTS

Lateral geniculate nucleus

In *Cebus*, the lateral geniculate nucleus (LGN), as illustrated in a coronal section stained by the Nissl method in Figure 1A, is formed by two magnocellular (M) layers in its more ventral portion (containing larger projection neurons) and four parvocellular (P) layers located dorsally (containing medium-sized neurons). In this species, as previously described by Hess and Edwards (1987), the P layers are not totally individualized and join each other in some portions of the nucleus. The reaction for SMI-32 in the LGN shows immunoreactive cells in both the P (Fig. 1D) and M (Fig. 1E) layers. In the M layers, however, labeling was more intense in terms of both a greater number of labeled cells and more intense staining of the neuropil (Fig. 1B,C). Rare cells were observed in the interlaminar and S layers (Fig. 1C). SMI-32-ir cells were mainly round or fusiform, with a pale nucleus and visible proximal dendrites (Fig. 1D,E).

Primary visual area (V1)

The distribution pattern of the neurofilament protein revealed by SMI-32 immunostaining in V1 of *Cebus* monkeys is illustrated in Figure 2A. Figure 2B shows an adjacent coronal section stained by the Nissl method; approximate limits of the layers are delineated. Brodmann's nomenclature was used throughout the text and figures to allow direct comparison with most previous works in Old World primates (Hof et al., 1996; Chaudhuri et al., 1996). The layers according to Hassler's nomenclature are cited in parentheses in the text.

The reaction for SMI-32 revealed a clear pattern of lamination with a large number of labeled cells and a

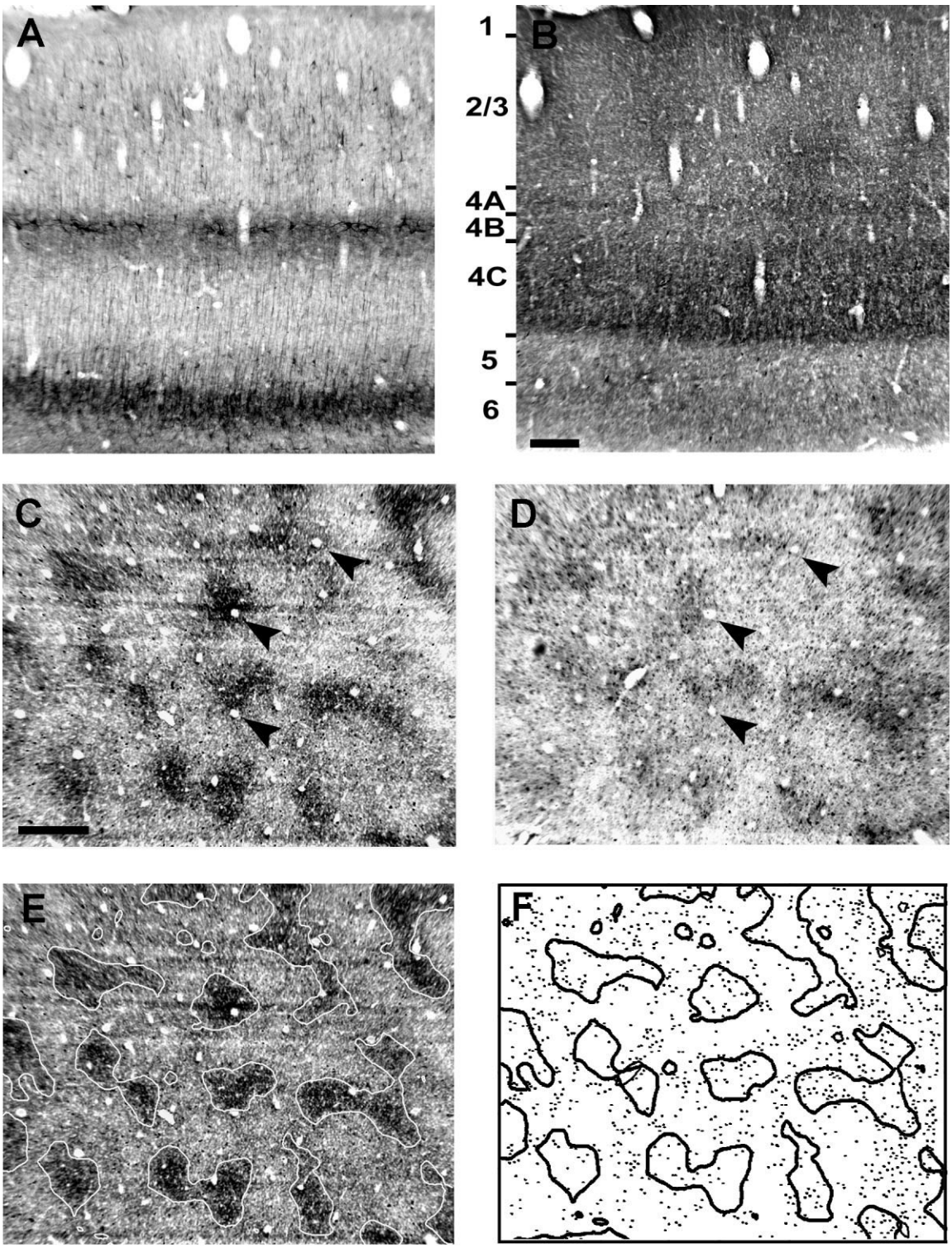

Fig. 4. **A,B:** Photomicrographs of adjacent coronal sections of V1 in *Cebus* reacted for SMI-32 immunocytochemistry (A) and for CO (B). **C,D:** Adjacent tangential sections showing the CO blob pattern (C) and SMI-32-ir cell distribution (D). Arrowheads point to the blood vessels used for alignment of sections. **E:** Same section shown in C, where the blobs of CO were automatically delineated (white contours) after the procedure described in Materials and Methods. **F:** Superposition of CO blobs (black contours) with SMI32-ir cells (dots) plotted in the section illustrated in D. Scale bar = 200 μm in B (applies to A,B); 300 μm in C (applies to C–F).

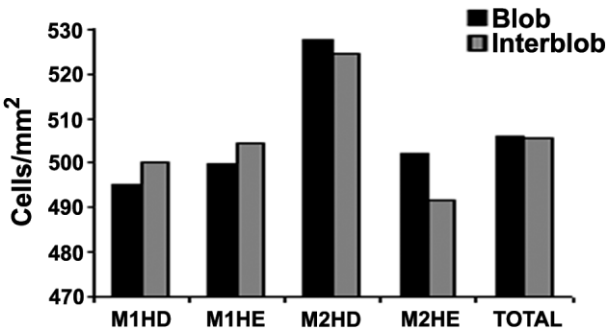

Fig. 5. SMI32-ir cell density in blob and interblob regions for four analyzed hemispheres. The rightmost histograms show the average cell density. No statistical difference (t-test, $P < 0.05$) was found for cell density in blob and interblob in any case.

heavily stained neuropil in layers 2/3 (3A), 4B (3C), and 6. Layer 5 showed a moderate staining of the neuropil, which consists mainly of apical dendrites of pyramidal cells located in layer 6. The geniculorecipient layers 4A (3B) and 4C (4) stained lightly for SMI-32. This pattern changed abruptly at the V1/V2 border (Fig. 3), where we observed not only an interruption of the heavy labeling in layers 4B and 6 but also an increase in the number of labeled pyramidal cells with large and intensely stained apical dendrites in layers 2/3 of V2.

A comparison of the distribution patterns of SMI-32 (Fig. 4A) and CO (Fig. 4B) in V1 demonstrates their complementary nature. The most heavily labeled layers for CO (layers 4A and 4C) are poorly labeled for SMI-32, whereas layer 4B and upper layer 6, which are heavily stained for SMI-32, are weakly labeled for CO. In layers 2/3, where the CO reaction shows densely stained regularly spaced blobs (Fig. 4C), the immunoreacted neuropil appears denser in the regions that correspond to CO blobs, and SMI-32-ir cells tend to form clusters (Fig. 4D). However, these SMI-32-ir cells are present both in CO blob and in interblobs regions, as evidenced by the superposition of adjacent tangent sections of V1, reacted for CO and for SMI-32, illustrated in Figure 4F. Figure 5 shows the SMI-32-ir cell density for each of the four hemispheres analyzed, as well as the mean density for the total area of blobs and interblobs. We did not observe a statistically significant difference (t-test, $P < 0.05$) in the SMI-32-ir cell mean density between blob and interblob regions.

The SMI-32-ir cells in layers 2/3 (Fig. 6A,B) are mainly small and lightly labeled pyramidal neurons with apical dendrites oriented toward layer 1, where we observe horizontally oriented labeled processes (Fig. 6A). A few labeled pyramidal neurons were found scattered in layers 4A and 4C. Layer 4B presents some pyramidal neurons and a net of darkly stained neuropil as well as a great number of large, darkly stained multipolar cells with intensely labeled dendrites oriented mainly horizontally (Fig. 6C,D). Elston and Rosa (1997) suggested that these large multipolar cells that project to area MT are in fact modified pyramidal cells. At the inferior border of layer 5 and superior half of layer 6, we observe dark labeled neuropil and a population of small pyramidal neurons with apical processes that cross layers 5 and 4C. In layer 6 we also observed very large cells with darkly stained apical dendrites and basal dendrites with extensive horizontal branching (Fig. 6E,F).

Area MT

In *Cebus*, MT is located in the posterior bank of the superior temporal sulcus (STS) and can be clearly characterized by a dense myelination (Fig. 7A), which extends from layer 6 to the bottom of layer 3 (Fiorani et al., 1989; Rosa et al., 1993). In Nissl-stained sections (Fig. 7C), MT presents a dense layer 6 and a sparser layer 4. The distribution of SMI-32-ir cells in MT of *Cebus* is illustrated in Figure 7B and D. When we compare the pattern of staining for SMI-32 in MT with that of surrounding areas, we can observe that MT shows a distinctive pattern with a dense band of labeled neuropil and large pyramidal neurons in layer 3 (Fig. 7E), sparse, very large, darkly labeled neurons in layer 5 (Fig. 7F), and a population of small and lightly labeled cells in layer 6 (Fig. 7G).

DISCUSSION

Previous studies have shown that the SMI-32 antibody labels preferentially cells related to the magnocellular pathway, at both thalamic and cortical levels (Campbell and Morrison, 1989; Hof and Morrison, 1995; Chaudhuri et al., 1996; Hof et al., 1996; Bourne and Rosa, 2003; Baldauf, 2005; Van der Gucht et al., 2005). In this study we showed that in the LGN of *Cebus* monkey, staining with SMI-32 labeled the magnocellular layer more intensely than the parvocellular ones, similar to what has been described in vervet monkey (Chaudhuri et al., 1996) and in marmoset (Bourne and Rosa, 2003). In V1 of *Cebus* layers 4B and 6, layers that project to area MT (Shipp and Zeki 1989; Callaway and Wiser, 1996), contain the largest and most intensely labeled SMI-32-ir neurons. In addition we showed that area MT can be characterized by strong labeling of the neuropil and by the presence of heavily labeled pyramidal cells in layers 3, 5, and 6. Thus, the higher level of neurofilament protein in neurons related to the magnocellular pathway can be considered as a common characteristic of all New and Old World primate species studied (macaque: Hof and Morrison, 1995; vervet: Chaudhuri et al., 1996; marmoset: Bourne and Rosa, 2003; Baldauf, 2005).

In the superficial layers of V1 in *Cebus*, our results do not suggest a correlation between the distribution of SMI-32-ir cells and the CO modules. This result is similar to that previously described in macaque monkey (Fenstemaker et al., 2001), in which SMI-32 immunoreactivity is distributed across the blob and interblob regions. In the squirrel monkey, however, Duffy and Livingstone (2003) found a greater density of SMI-32-labeled neurons in the interblob regions than within the blobs. These authors suggested that this difference may be the consequence of the more distinct blob patterns that exist in squirrel monkeys compared with macaques. However, *Cebus* monkeys have well-delimited CO blobs, which tend to be more individualized than those described in macaque, although less defined than those described in squirrel monkey (Rosa et al., 1991). The presence of SMI-32-ir neurons within both blob and interblob regions is consistent with recent findings that parvo- and magnocellular channels intermingle in superficial layers of V1, in which both CO blobs and interblobs receive magno inputs from layers 4Cα and 4B and parvo inputs from layer 4Cβ (Lachica et al., 1992;

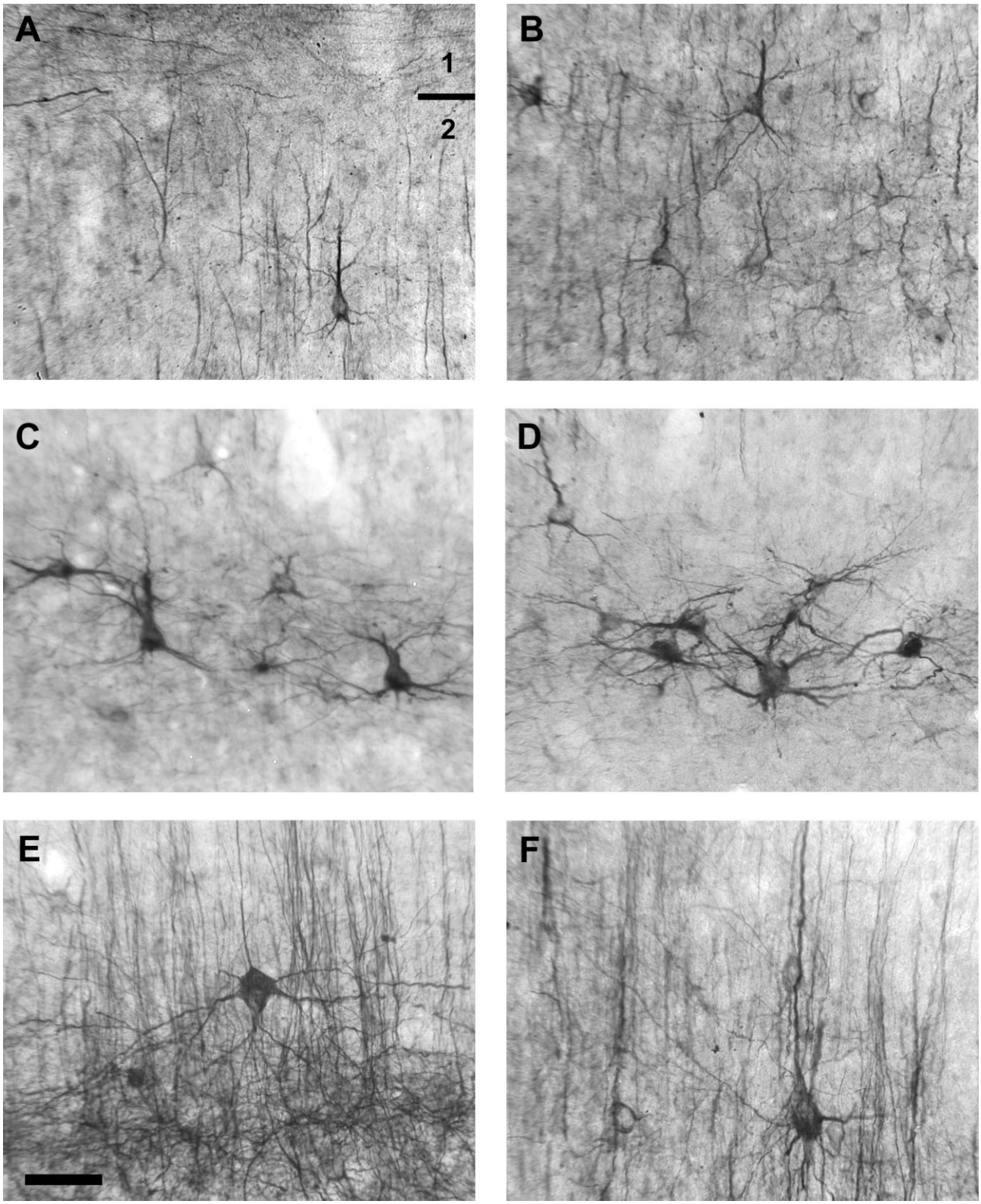

Fig. 6. Photomicrographs of SMI-32-ir cells and neuropil in layers 1 and 2 (**A**), 2/3 (**B**), 4B (**C,D**), and 6 (**E,F**) in V1 in *Cebus* monkey. Scale bar = 50 μm in E (applies to A–F).

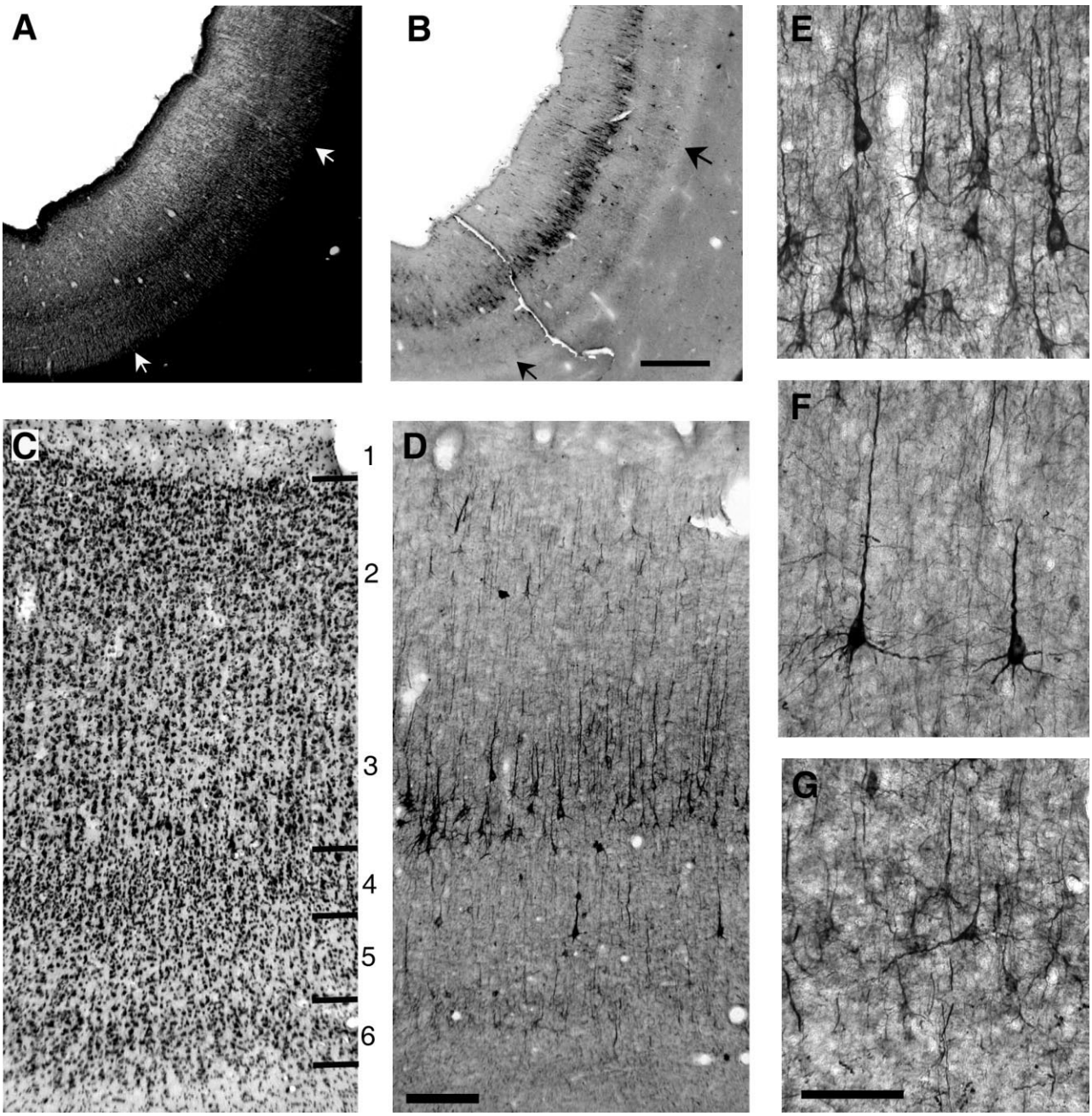

Fig. 7. Photomicrographs of parasagittal sections of the posterior bank of the STS, at the level of area MT of *Cebus*. **A:** Myelin-stained section showing the borders of area MT revealed by its dense myelination pattern (arrows). **B:** Section adjacent to that illustrated in A reacted for SMI-32, showing an intense reaction in the neuropil and cells in layer 3 and labeled cells in layers 5 and 6. **C,D:** Adjacent sections stained for Nissl (C) and SMI-32 (D) showing the laminar patterns in area MT. **E–G:** Enlarged photomicrographs show SMI-32-ir cells in layers 3 (E), 5 (F), and 6 (G). Scale bar = 1 mm in B (applies to A,B); 200 μm in D (applies to C,D); 100 μm in G (applies to E–G).

Yoshioka et al., 1994; Callaway and Wiser, 1996). In addition, a strict segregation of the blob and interblob projections to different V2 compartments has been questioned (Sincich and Horton, 2002; Xiao and Felleman, 2004).

Hof et al. (1996) analyzed the distribution of neurofilament protein-immunoreactive neurons following injections of retrograde tracers and showed that feedforward connections to areas MT and V4 are characterized by distinct neurochemical features. The projections to MT contained consistently higher numbers of SMI-32-ir neurons (78%) than the projections to area V4 (32%). Among the projections to area MT, 100% of the retrogradely labeled cells in layer 4B and the Meynert cells in area V1

were also neurofilament protein-immunoreactive. The presence of neurofilament protein has been correlated with stabilization of the axonal cytoskeleton in large neurons with high conduction velocity, an important cellular feature in detection of movement (Campbell et al., 1991; Hof and Morrison, 1995). Our data in *Cebus* corroborate these ideas: strong labeling is seen for SMI-32 in layers 4B and 6 in V1, layers that project directly to MT (Rosa et al., 1993), an area that presents a systematic organization for direction of motion selectivity (Zeki, 1974; Albright, 1984; Diogo et al., 2002, 2003). Nonetheless, further studies are needed to clarify the role of SMI-32-ir cells in layers 2/3 of V1.

In this study we showed that the distribution pattern of neurofilament proteins in *Cebus* is more comparable to that of the *Macaca*, an Old World monkey, than to that of the squirrel monkey, another New World monkey. In spite of being widely separated in evolutionary terms (Preuss and Goldman-Rakic, 1991), *Cebus* and *Macaca* show various similarities, as described in previous works (Gattass and Gross, 1981; Gattass et al., 1981, 1987, 2005; Rosa et al., 1988; Fiorani et al., 1989; Padberg et al., 2007). Padberg and collaborators (2007) have suggested epigenetic mechanisms to explain the parallel emergence of some anterior parietal areas in both species. In relation to the similarity in the distribution pattern of neurofilament proteins in these species, it seems that it can also be due to epigenetic factors that promote common developmental mechanisms in individuals that have similar characteristics and a similar ecological niche.

ACKNOWLEDGMENTS

The authors are grateful to Dr. A P.B. Souza for comments on the manuscript, to E.S. da Silva Filho, L.H. Pontes, and M.T. Monteiro for technical assistance, and to P. Coutinho and G. Coutinho for animal care.

LITERATURE CITED

Albright TD. 1984. Direction and orientation selectivity of neurons in visual area MT of the macaque. J Neurophysiol 52:1106–1130.

Baldauf ZB. 2005. SMI-32 parcellates the visual cortical areas of the marmoset. Neurosci Lett 383:109–114.

Bourne JA, Rosa MGP. 2003. Neurofilament protein expression in the geniculostriate pathway of a New World monkey (*Callithrix jacchus*). Exp Brain Res 150:19–24.

Bourne JA, Warner CE, Upton DJ, Rosa MGP. 2007. Chemoarchitecture of the middle temporal visual area in the marmoset monkey (*Callithrix jacchus*): laminar distribution of calcium-binding proteins (calbindin, parvalbumin) and nonphosphorylated neurofilament. J Comp Neurol 500:832–849.

Callaway EM, Wiser AK. 1996. Contributions of individual layer 2–5 spiny neurons to local circuits in macaque primary visual cortex. Vis Neurosci 13:907–922.

Campbell MJ, Morrison JH. 1989. Monoclonal antibody to neurofilament protein (SMI-32) labels a subpopulation of pyramidal neurons in the human and monkey neocortex. J Comp Neurol 282:191–205.

Campbell MJ, Hof PR, Morrison JH. 1991. A subpopulation of primate corticocortical neurons is distinguished by somatodendritic distribution of neurofilament protein. Brain Res 539:133–136.

Chaudhuri A, Zangenehpour S, Matsubara JA, Cynader MS. 1996. Differential expression of neurofilament protein in the visual system of the vervet monkey. Brain Res 709:17–26.

Diogo ACM, Soares JGM, Albright TD, Gattass R. 2002. Two-dimensional map of direction selectivity in cortical visual area MT of *Cebus* monkey. An Acad Bras Cienc 74:463–476.

Diogo ACM, Soares JGM, Koulakov A, Albright TD, Gattass R. 2003. Eletrophysiological imaging of functional architecture in the cortical middle temporal visual area of *Cebus apella* monkey. J Neurosci 23: 3881–3898.

Duffy KR, Livingstone MS. 2003. Distribution of non-phosphorylates neurofilament in squirrel monkey V1 is complementary to the pattern of cytochrome-oxidase blobs. Cereb Cortex 13:722–727.

Elston GN, Rosa MGP. 1997. The occipitoparietal pathway of the macaque monkey: comparison of pyramidal cell morphology in layer III of functionally related cortical visual areas. Cereb Cortex 7:432–452.

Fenstemaker SB, Kiorpes L, Mosvshon JA. 2001. Effects of experimental strabismus on the architecture of macaque monkey striate cortex. J Comp Neurol 438:300–317.

Fiorani JR M, Gattass R, Rosa MGP, Sousa APB. 1989. Visual area MT in the *Cebus* monkey: location, visuotopic organization, and variability. J Comp Neurol 287:98–118.

Fries W, Keizer K, Kuypers HG. 1985. Large layer VI cells in macaque striate cortex (Meynert cells) project to both superior colliculus and prestriate visual area V5. Exp Brain Res 58:613–616.

Gallyas F. 1979. Silver staining of myelin by means of physical development. Neurol Res 1:203–209.

Gattass R, Gross CG. 1981. Visual topography of the striate projection zone in the posterior superior temporal sulcus (MT) of the macaque. J Neurophysiol 46:621–638.

Gattass R, Gross CG, Sandell JH. 1981. Visual topography of V2 in the macaque. J Comp Neurol 201:519–539.

Gattass R, Sousa APB, Rosa MGP. 1987. Visual topography of V1 in the *Cebus* monkey. J Comp Neurol 259:529–548.

Gattass R, Nascimento-Silva S, Soares JGM, Lima B, Jansen AKA, Diogo ACM, Fiorani M. 2005. Cortical visual areas in monkeys: location, topography, connections, columns, plasticity and cortical dynamics. Philos Trans R Soc Lond B Biol Sci 360:709–731.

Hendrickson AE, Wilson JR, Ogren MP. 1978. The neuroanatomical organization of pathways between the dorsal lateral geniculate nucleus and visual cortex in Old World and New World primates. J Comp Neurol 182:123–136.

Hess DT, Edwards MA. 1987. Anatomical demonstration of ocular segregation in the retinogeniculocortical pathway of the New World capuchin monkey (*Cebus apella*). J Comp Neurol 264:409–420.

Hof PR, Morrison JH. 1990. Quantitative analysis of vulnerable subset of pyramidal neurons in Alzheimer's disease: II. Primary and secondary visual cortex. J Comp Neurol 301:55–64.

Hof PR, Morrison JH. 1995. Neurofilament protein defines regional patterns of cortical organization in the macaque monkey visual system: a quantitative immunohistochemical analysis. J Comp Neurol 352:161–186.

Hof PR, Ungerleider LG, Webster MJ, Gattass R, Adams MM, Sailstad CA, Morrison JH. 1996. Neurofilament protein is differentially distributed in subpopulations of corticocortical projection neurons in the macaque monkey visual pathways. J Comp Neurol 376:112–127.

Kaas JH, Huerta MF, Weber JT, Harting JK. 1978. Patterns of retinal terminations and laminar organization of the lateral geniculate nucleus of primates. J Comp Neurol 182:517–553.

Lachica EA, Beck PD, Casagrande VA. 1992. Parallel pathways in macaque monkey striate cortex: anatomically defined columns in layer III. Proc Natl Acad Sci U S A 89:3566–3570.

Padberg J, Franca JG, Cooke DF, Soares JGM, Rosa MGP, Fiorani M, Gattass R, Krubitzer L. 2007. Parallel evolution of cortical areas involved in skilled hand use. J Neurosci 27:10106–10115.

Preuss TM, Goldman-Rakic PS. 1991. Architectonics of the parietal and temporal association cortex in the strepsrhine primate *Galago* compared to the anthropoid primate *Macaca*. J Comp Neurol 310:475–506.

Rosa MGP. 2002. Visual maps in the adult primate cerebral cortex: some implications for brain development and evolution. Braz J Med Biol Res 35:1485–1498.

Rosa MGP, Sousa APB, Gattass R. 1988. Representation of the visual field in the second visual area in the *Cebus* monkey. J Comp Neurol 275: 326–345.

Rosa MGP, Gattass R, Soares JGM. 1991. A quantitative analysis of cytochrome oxidase-rich patches in the primary visual cortex of *Cebus* monkeys: topographic distribution and effects of late monocular enucleation. Exp Brain Res 84:195–209.

Rosa MGP, Soares JGM, Fiorani M, Gattass R. 1993. Cortical afferents of visual area MT in the *Cebus* monkey: possible homologies between New and Old World monkeys. Vis Neurosci 10:827–855.

Shipp S, Zeki S. 1989. The organization of connections between areas V5 and V1 in macaque monkey visual cortex. Eur J Neurosci 1:309–332.

Silverman MS, Tootell RBH. 1987. Modified technique for cytochrome oxidase histochemistry: increased staining intensity and compatibility with 2-deoxyglucose autoradiograph. J Neurosci Methods 19:1–10.

Sincich LC, Horton JC. 2002. Divided by cytochrome oxidase: a map of the projections from V1 to V2 in macaques. Science 295:1734–1737.

Spatz WB. 1977. Topographically organized reciprocal connections between areas 17 and MT (visual area of the superior temporal sulcus) in the marmoset *Callithrix jacchus*. Exp Brain Res 27:559–572.

Spatz WB. 1978. The retino-geniculo-cortical pathway in *Callithrix*. I. Intraspecific variations in the lamination pattern of the lateral geniculate nucleus. Exp Brain Res 33:551–563.

Sternberger LA, Sterberger NH. 1983. Monoclonal antibodies distinguish phosphorylated and nonphosphorylated forms of neurofilaments in situ. Proc Natl Acad Sci U S A 80:6126–6130.

Van der Gucht E, Clerens S, Jacobs S, Arckens L. 2005. Light-induced Fos expression in phosphate-activated glutaminase- and neurofilament protein-immunoreactive neurons in cat primary visual cortex. Brain Res 1035:60–66.

Van de Gucht E, Youakim M, Arckens L, Hof PR, Baizer JS. 2006. Variations in the structure of the prelunate gyrus in Old World monkeys. Anat Rec A:753–775.

Xiao Y, Felleman DJ. 2004. Projections from primary visual cortex to cytochrome oxidase thin stripes and interstripes of macaque visual area 2. Proc Natl Acad Sci U S A 101:7147–7151.

Yoshioka T, Levitt JB, Lund JS. 1994. Independence and merger of thalamocortical channels within macaque monkey primary visual cortex: anatomy of interlaminar projections. Vis Neurosci 11:467–489.

Zeki, SM. 1974. Functional organization of a visual area in the posterior bank of the superior temporal sulcus of the rhesus monkey. J Physiol 236:549–573.